Oncogene
https://doi.org/10.1038/s41388-019-1129-3

ARTICLE

Plakophilin 1 enhances MYC translation, promoting squamous cell lung cancer

Joel Martin-Padron[1,2,3] · Laura Boyero[1,2] · Maria Isabel Rodriguez[1,4] · Alvaro Andrades[1,4] · Inés Díaz-Cano[1,2,3] · Paola Peinado[1,4] · Carlos Baliñas-Gavira[1,4] · Juan Carlos Alvarez-Perez[1,4] · Isabel F. Coira[1,4] · María Esther Fárez-Vidal[2,3] · Pedro P. Medina[1,3,4]

Received: 2 September 2019 / Revised: 6 November 2019 / Accepted: 20 November 2019

Abstract

Plakophilin 1 (PKP1) is a member of the arm-repeat (armadillo) and plakophilin gene families and it is an essential component of the desmosomes. Although desmosomes have generally been associated with tumor suppressor functions, we have consistently observed that PKP1 is among the top overexpressed proteins in squamous cell lung cancer. To explore this paradox, we developed in vivo and in vitro functional models of PKP1 gain/loss in squamous cell lung cancer. CRISPR-Cas9 PKP1 knockout severely impaired cell proliferation, but it increased cell dissemination. In addition, PKP1 overexpression increased cell proliferation, cell survival, and in vivo xenograft engraftment. We further investigated the molecular mechanism of the mainly oncogenic function of PKP1 by combining transcriptomics, proteomics, and protein-nucleic acid interaction assays. Interestingly, we found that PKP1 enhances *MYC* translation in collaboration with the translation initiation complex by binding to the 5′-UTR of *MYC* mRNA. We propose PKP1 as an oncogene in SqCLC and a novel posttranscriptional regulator of MYC. PKP1 may be a valuable diagnostic biomarker and potential therapeutic target for SqCLC. Importantly, PKP1 inhibition may indirectly target MYC, a primary anticancer target.

Introduction

Lung cancer is the leading cause of cancer mortality, due its high incidence and mortality rate. The direct healthcare costs of this disease were reported to be 12.1 billion USD/year in the USA alone [1]. Despite diagnostic improvements and therapeutic advances, lung cancer remains highly lethal, and only about 18% of patients in developed countries remain alive at 5 years post diagnosis [2]. Standard therapeutic strategies such as surgery, chemotherapy, or radiotherapy appear to have reached a plateau [3]. Furthermore, genetic alterations have been associated with the development and progression of lung cancer, but the underlying molecular mechanisms remain unclear [4, 5].

Numerous laboratories, including our own, conduct systematic gene expression analysis in tumors to detect any gene that may be involved in carcinogenesis. However, the biological implications of aberrant tumor gene expression are poorly understood, and meaningful functional experiments are needed to select potential candidates for the development of novel tumor markers and anticancer drugs. Interestingly, in two independent studies [6, 7], our group

Lead contact: Pedro P. Medina

These authors contributed equally: Joel Martin-Padron, Laura Boyero

Supplementary information The online version of this article (https://doi.org/10.1038/s41388-019-1129-3) contains supplementary material, which is available to authorized users.

✉ María Esther Fárez-Vidal
efarez@ugr.es

✉ Pedro P. Medina
pedromedina@ugr.es

1 Centre for Genomics and Oncological Research (GENYO), Granada, Spain

2 Department of Biochemistry and Molecular Biology III, University of Granada, Granada, Spain

3 Institute for Biomedical Research ibs. Granada, University Hospital Complex of Granada/University of Granada, Granada, Spain

4 Department of Biochemistry and Molecular Biology I, University of Granada, Granada, Spain

Published online: 10 December 2019

observed consistent and frequent overexpression of the gene encoding plakophilin 1 (PKP1) in squamous cell lung carcinoma (SqCLC), which is a major subtype of nonsmall cell lung cancer (NSCLC) and accounts for around 30% of all lung tumors [8].

PKP1 is a member of the plakophilin family of proteins, which are mainly expressed by cells of stratified and single-layered epithelia. Plakophilins belong to the p120-catenin subfamily of armadillo-domain proteins and provide physical links between selectively synthesized desmosomal proteins [9]. Decreased assembly of desmosomes has been reported in several epithelial cancers. Multiple authors have described a role for desmosomes in tumor suppression, reporting that their downregulation drives tumor development and early invasion [10, 11]. Furthermore, plakophilin expression has been correlated with desmosome instability, decreased cell adhesion, increased cell migration, and a poor prognosis [12]. However, our observations of *PKP1* overexpression in SqCLC do not support these previous reported data. In the present study, we developed in vitro and in vivo functional models of PKP1 gain/loss in order to explore the specific function of PKP1 in lung cancer. Although increased cell dissemination was displayed by CRISPR-Cas9 PKP1-knockout clones, PKP1 evidenced a pro-oncogenic role in other experiments as a promoter of cell proliferation, cell survival, and xenograft engraftment. An important finding was that these pro-oncogenic activities are mediated by the functional relationship of PKP1 with MYC. These new mechanistic observations reveal *PKP1* as a novel oncogene in SqCLC, and as an effective posttranscriptional regulator of *MYC*, which has been found overexpressed in around 70% of NSCLC tumors [13].

Results

PKP1 is among the most overexpressed genes in squamous cell lung cancer (SqCLC)

In a previous study using first-generation competitive hybridization expression microarrays (dataset GSE8569), we found *PKP1* to be the most overexpressed gene in SqCLC ($n = 36$) vs. normal lung tissue ($n = 6$) samples, with a mean fold change of 22.5 [6]. In a subsequent investigation using a different microarray hybridization technology, we consistently observed *PKP1* overexpression in an independent set of 21 SqCLC tumors (dataset GSE18842), and *PKP1* was again among the most overexpressed genes in SqCLC ($n = 21$) vs. normal lung tissue ($n = 22$) samples, with a fold change of 112 ($p = 0.00017$) [7].

These observations have been validated also with external datasets with a higher sample size (GSE19188, GSE3526, and TCGA-LUAD-TCGA-LUSC) [14–16]

Detailed statistical analysis comparing *PKP1* levels in the two major NSCLC (SqCLC and LUAD) and their nontumoral controls in the five cited datasets (total $n = 1521$) confirmed that *PKP1* is consistently and very significantly overexpressed in SqCLC when compared with LUAD and to normal lung tissue (Fig. S1A). This observation was found in all the datasets independently of the method used for measuring gene expression (different microarrays platforms or RNA-seq) (Table S1). As example, in the larger dataset (TCGA), the *PKP1* fold change between SqCLC ($n = 501$) and LUAD ($n = 515$) was 80.81, and extremely significant ($p < 2.2 \times 10^{-16}$); and the *PKP1* fold change between SqCLC ($n = 501$) and nontumoral controls ($n = 51$) was 53.59, and also extremely significant ($p < 2.2 \times 10^{-16}$).

However, these observations of *PKP1* overexpression have not been studied in detail in SqCLC, probably because it appear to contradict current assumptions about the biological function of PKP1 as desmosome component. Thus, desmosomes have been reported to possess tumor suppressor properties by promoting cell-to-cell cohesion and restricting cell mobility [11]. We developed the functional models described below to address this apparent paradox and gain insight into the biological role of PKP1 in lung cancer.

PKP1 knockdown reduces cell viability and proliferation and enhances apoptosis

Loss-of-function studies were performed in a PKP1-overexpressing SqCLC cell line to assess the possible role of PKP1 in the growth or survival of lung cancer cells. For the selection of a cell line model, we based on a previous publication [17] that found the SK-MES-1 cells expressing high levels of PKP1 transcript on an analysis of desmosomal proteins in eight SqCLC cell lines. SK-MES-1 cell line was acquired from the ATTC and PKP1 expression levels were proved high. The PKP1 protein has two splice isoforms (PKP1a and PKP1b) [18]. Sequencing of the PKP1 transcripts in SK-MES-1 cells revealed expression of PKP1a isoform alone, which displayed no mutations (Fig. S1B). PKP1 isoform "b" was not detected in NSCLC cell lines or in tissue samples from NSCLC or normal lung (Fig. S1C).

Two siRNAs targeting PKP1 (siRNA-1, siRNA-2) were tested at different concentrations and time intervals to develop PKP1-knockdown assays. Effective downregulation of PKP1 protein expression was achieved by a combination of the two PKP1-specific siRNAs, as

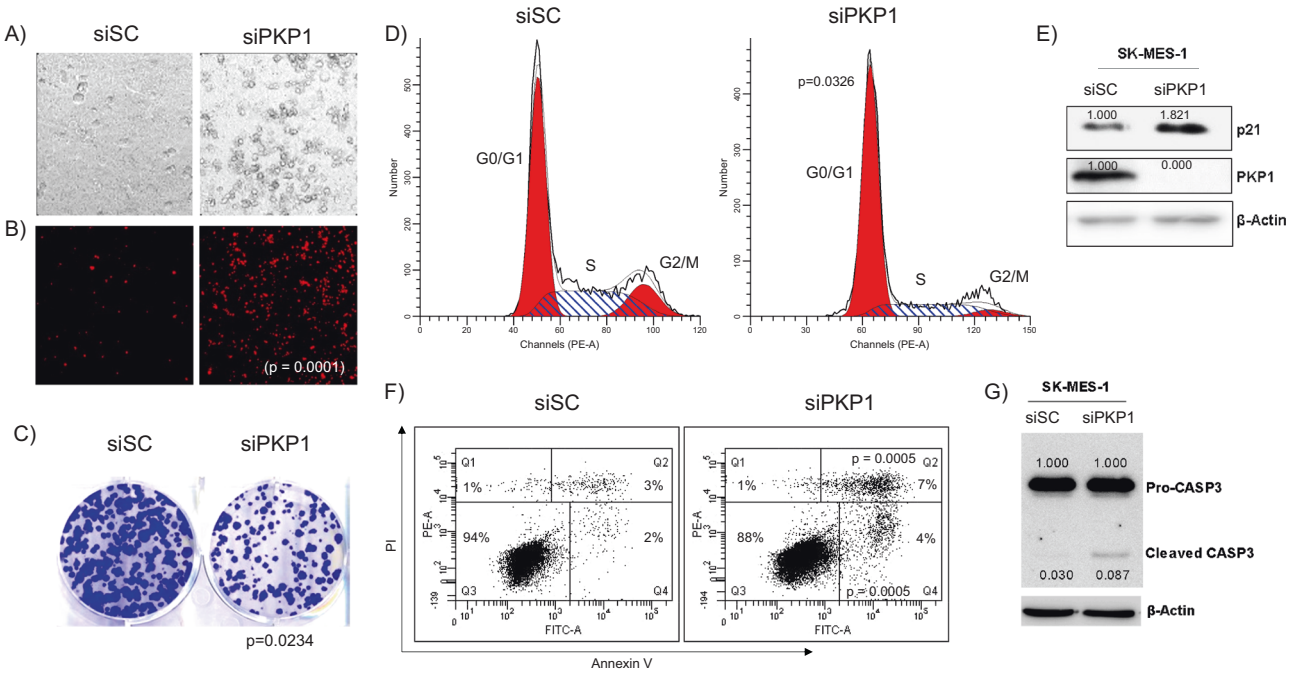

Fig. 1 Morphology, viability, cell-colony analysis, cell cycle progression, p21 expression, and apoptosis determination of SK-MES-1 cells after PKP1 silencing. a Live microscopic examination revealed higher number of cells with spherical morphology 48–72 h post transfection. **b** Propidium iodide (PI) staining at 72 h post transfection, showing 4.5-fold higher PI-positive (PI+) cell rate vs. scrambled-siRNA controls ($p = 0.0001$). **c** Cell colony formation analysis at 3 weeks revealed significant fewer colonies in knockdown vs. control wells ($p = 0.0234$). **d** Flow cytometry analysis of cell cycle progression: graphic representation of changes in cell cycle profile at 72 h of treatment. PKP1 silencing produced a significant increase in the percentage of cells in G0/G1 at 72 h ($p = 0.0326$) suggesting a cell cycle arrest on this phase. **e** Western blot assay of p21 protein levels showed an increase in PKP1 knockdown vs. control cells at 72 h (1.821-fold change). **f** Graphic representation of Annexin V-positive cell analysis at 72 h of treatment, showing >2.5-fold higher early apoptosis rate (4% of total cells) ($p = 0.0005$) (Q4) and ~60% increase in late apoptosis rate (7% of total cells) ($p = 0.0005$) (Q2). **g** Western blot results for procaspase-3 expression and cleaved caspase-3 in SK-MES-1 cells, evidencing caspase-3 activation (approximately threefold than control) at 72 h post transfection in cells treated with siRNAs against PKP1. siPKP1, Knockdown siRNA-1 against PKP1 plus siRNA-2 against PKP1; siSC, scrambled-siRNA control; G1, gap 1 cell cycle phase; S, synthesis cell cycle phase; G2, gap 2 cell cycle phase. Annexin V-FITC-A, Annexin V linked to fluorescein isothiocyanate; PI PE-A, propidium iodide stain; Q1, cell death; Q2, late apoptosis; Q3, living cells; Q4, early apoptosis. PKP1, plakophilin 1; p21, cyclin-dependent kinase inhibitor 1A; B-actin, beta-actin; Pro-Caspase 3, inactive apoptosis-related cysteine peptidase; Caspase 3, active apoptosis-related cysteine peptidase.

confirmed by real-time PCR and western blot assays (Fig. S2A, B).

Microscopic in vivo examination of PKP1-silenced SK-MES-1 cells revealed a significantly higher number of cells with spherical morphology at 48–72 h post transfection (SVideo 1, Fig. 1a). The viability of these spherical cells was tested by propidium iodide (PI) staining at 72 h post transfection. A 4.5-fold higher PI-positive rate was found for PKP1 knockdown cells vs. scrambled-siRNA controls ($p = 0.0001$) (Fig. 1b), indicating that cell viability was significantly impaired by PKP1 knockdown. Cell proliferation ($p = 0.0348$) (Fig. S2C) and cell-colony formation ($p = 0.0234$) (Fig. 1c) assays showed that both were significantly reduced in PKP1 knockdown cells vs. respective negative controls. We then explored possible mechanisms underlying the decrease in SK-MES-1 cell proliferation after PKP1 expression loss. Thus, flow cytometry studies were conducted to determine whether this loss inhibited cell cycle progression and/or affected apoptosis. PKP1 silencing impaired cell cycle progression and significantly increased the percentage of cells in G0/G1 cell cycle phase ($p = 0.0326$) (Figs. 1d, S2D). The cell cycle arrest was further investigated by western blot analysis of the expression of p21, which functions as a regulator of cell cycle progression at G1, revealing an appreciable (1.82 fold change) increase in p21 protein accumulation due to PKP1 knockdown (Fig. 1e). In a subsequent exploration of the role of apoptosis, the percentage of Annexin V-positive cells was found to be increased by PKP1 expression loss (Figs. 1F, S2E), with a ~2.5-fold higher early apoptosis rate (4% of total cells) ($p = 0.0005$) and ~60% higher late apoptosis rate (7% of total cells) ($p = 0.0005$). Expression of activated caspase-3, the effector caspase of apoptotic cell death, was studied by immunoblotting, finding that PKP1 silencing promoted the proteolytic cleavage of procaspase-3 (approximately threefold than control), triggering the execution phase of apoptosis (Fig. 1g).

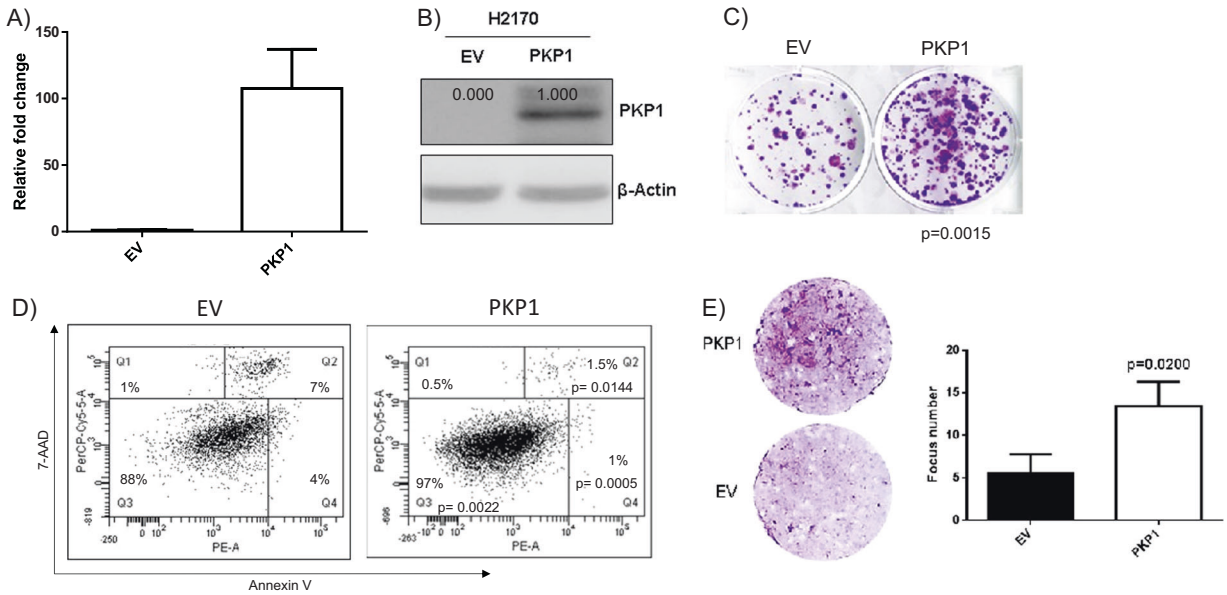

Fig. 2 Ectopic expression of PKP1 in NCI-H2170 SqCLC cell line after pLVX-IRES-ZsGreen1-PKP1A plasmid transduction. a qPCR analysis of relative *PKP1* mRNA expression at 72 h of treatment indicates successful transduction. **b** Western blot analysis at 72 h of transduction confirms ectopic PKP1 expression. **c** Clonogenic assay at 3 weeks, revealing a significant increase in the number and size of colonies after ectopic PKP1 expression ($p = 0.0015$); three biological replicates are represented. **d** Graphic representation of Annexin-V assay at 72 h after ectopic PKP1 expression, showing a significantly increased percentage of viable cells (97% of cells) ($p = 0.0022$) (Q3) and significantly decreased percentage of early apoptotic ($p = 0.0005$) (1% of cells) (Q4) and late apoptotic (1.5% of cells) ($p = 0.0144$) (Q2) cells. **e** NIH 3T3 focus assay at 30 days, revealing a significant increase ($p = 0.0200$) in the number and size of colonies after ectopic PKP1 expression; three biological replicates are represented. EV, pLVX-IRES-ZsGreen1 empty vector; PKP1, pLVX-IRES-ZsGreen1-PKP1A isoform; B-Actin, beta-actin; PKP1, plakophilin 1; Annexin-V PE-A, Annexin-V linked to R-phycoerythrin; 7-AAD PerCP-Cy 5–5-A, 7-aminoactinomycin D stain; Q1, cell death; Q2, late apoptosis; Q3, living cells; Q4, early apoptosis; NIH 3T3, murine fibroblast cell line.

According to the above findings, PKP1 depletion suppresses cell growth and promotes apoptosis in the SqCLC cell line.

PKP1 ectopic expression enhances cell proliferation

The proliferative activity of PKP1 and its functional effect on lung cancer regulation were studied by expressing PKP1 ectopically in the NCI-H2170 SqCLC cell line, selected for its reported lack of PKP1 expression [17]. PKP1 was cloned into the lentiviral pLVX-IRES-ZsGreen1 vector (Clontech, CA, USA). After NCI-H2170 transduction, PKP1 expression was tested by qPCR and western blot assays (Figs. 2a, b and S2F). Confocal microscopy confirmed that the cellular distribution of transduced PKP1 in NCI-H2170 was similar to endogenous PKP1 found in SK-MES-1 and EPLC-272H cell lines (Fig. S3A). In agreement with the PKP1 knockdown experiments, assay results showed that ectopic PKP1 expression in NCI-H2170 significantly promoted cell proliferation ($p = 0.0005$) (Fig. S2C) and colony formation ($p = 0.0015$) (Fig. 2c). Annexin-V assays revealed a significantly increased percentage of viable cells (97% of total cells) ($p = 0.0022$) and a significantly reduced percentage of early apoptotic (1% of total cells) ($p = 0.0005$) and late apoptotic (1.5% of total cells) ($p = 0.0144$) cells (Fig. 2d).

In order to confirm the oncogenic effect of PKP1 overexpression, we developed focus formation assays (Fig. 2e) on NIH 3T3 murine fibroblast. NIH 3T3 cells typically form a monolayer in culture. However, an oncogenic stimulus can cause multilayered grow and foci formation that can be stained by crystal violet in order to be quantified. Historically these analyses have been key to determine the oncogenicity of important oncogenes like RAS [19]. The result evidences a significant increment in focus formation caused by PKP1 ectopic expression ($p = 0.0200$) confirming the oncogenic role of PKP1 overexpression, at least in this context.

PKP1 knockout enhances cell dissemination but reduces cell proliferation

The functional role of PKP1 in SqCLC was explored by developing PKP1 knockout clones in the SK-MES-1 cell line using the CRISPR-Cas9 system. Two biallelic knockout clones with no PKP1 expression were obtained: PKP1-knockout clone #1, with homozygous deletion of nucleotide "C"; and PKP1-knockout clone #2, with deletion of nucleotide "C" in one allele and deletion of ten nucleotides "ACGGGGCACC" in the other (Fig. S3B, C). These genetic alterations were all located at the nucleotides targeted by the PKP1 sgRNA designed at exon 3 and produced

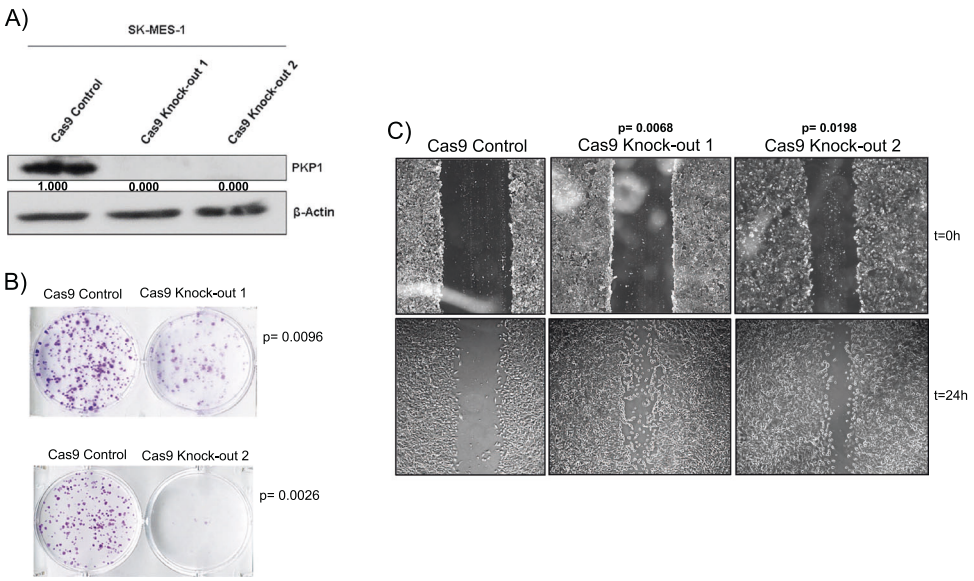

Fig. 3 Analysis of knockout clones #1 and #2 in SK-MES-1 cell line using the CRISPR-Cas9 system. a Western blot assay showed no wild-type PKP1 expression after targeting with CRISPR-Cas9 technology. **b** Clonogenic assay of knockout clones #1 ($p = 0.0096$) and #2 ($p = 0.0026$) at 3 weeks showed a significant reduction in the number and size of colonies vs. controls; three biological replicates are represented. **c** In vitro scratch assay of knockout clone #1 and #2 in SK-MES-1 cell line using CRISPR-Cas9 system, showing enhanced cell migration in knockout clone #1 ($p = 0.0068$) and #2 ($p = 0.0198$) vs. control, in three separate experiments. Cas9 Control, pspcas9(bb)-2a-puro empty vector-treated SK-MES-1 clonal cell line; Cas9 Knock-Out 1, pspcas9(bb)-2a-puro sgRNA against PKP1 exon 3 treated SK-MES-1 clonal cell line 1; Cas9 Knock-Out 2, pspcas9(bb)-2a-puro sgRNA against PKP1 exon 3 treated SK-MES-1 clonal cell line 2; PKP1, plakophilin 1; B-Actin, beta-actin.

translational frameshift and a premature stop codon (Fig. S4). No wild-type PKP1 expression was detected by western blot in either PKP1-knockout clones (Fig. 3a). Cell proliferation ($p = 0.0001$ for both clones) (Fig. S2C) and colony formation ($p = 0.0096$ for clone #1 and $p = 0.0026$ for clone #2) (Fig. 3b) were significantly reduced in PKP1-knockout #1 and #2 clones in comparison with their respective controls. The in vitro scratch assay [20] was used to study cell migration in these clones, finding a significant increase in cell migration vs. controls ($p = 0.0068$ for clone #1 and $p = 0.0198$ for clone #2) (Fig. 3c).

Intriguingly, the above results obtained in knockout clones indicate that PKP1 may possess both tumor-suppressor and oncogenic activities. Thus, PKP1 knockouts not only showed significantly lower proliferation, but also significantly higher cell migration. Next, we developed in vivo xenografts for the comparative evaluation of PKP1 tumor-suppressor and oncogenic effects in SK-MES-1 PKP1-knockout clones.

PKP1 knockout impairs tumor xenograft engraftment and cell growth

Tumor xenograft assays of PKP1-knockout cells were performed in immunodeficient NSG mice, using SK-MES-1 cells modified with the CRISPR-Cas-9 gene-editing system. Experimental cells were SK-MES-1 PKP1-knockout clones #1, while control cells were SK-MES-1 clones, with an empty cassette for the sgRNA. Experimental and control cells were transduced with luciferase (pUltra-chili-luc, Addgene #48688) to facilitate study of tumors derived from xenografts with the in vivo imaging system (IVIS). Equivalent transfection efficiency was determined by flow cytometry using the dTomato reporter, and the behavior of the tumor was followed in vivo according to its firefly luciferase expression.

Experimental and control groups of mice ($n = 10$ each) were tail-vein injected with 0.2 million cells. IVIS results revealed tumor cells in the lungs of both groups immediately after their inoculation. The in vivo luminescence of tumors was studied with IVIS at days 1, 4, 9, 15, and 24, observing a strong decay in the luminescence of xenografts from PKP1-knockout cells over time and an increase in the luminescence of those from PKP1-expressing cells ($p = 0.0016$) (Fig. 4a). In fact, the luminescence of xenografts from PKP1-knockout cells decayed so rapidly post inoculation that it was not possible to properly evaluate whether their dissemination was greater than that of PKP1-expressing cells.

Both groups of mice were sacrificed at day 24, extracting their organs and measuring their luminescence ex vivo. The luminescence was mainly observed in the lungs, where it was considerably increased in mice with PKP1-expressing clones and barely detectable in those with PKP1-knockout cells (Fig. 4b). Macroscopically, the lung surface in PKP1-expressing xenografts appeared granulated in comparison with the nearly smooth surface in PKP1-knockout

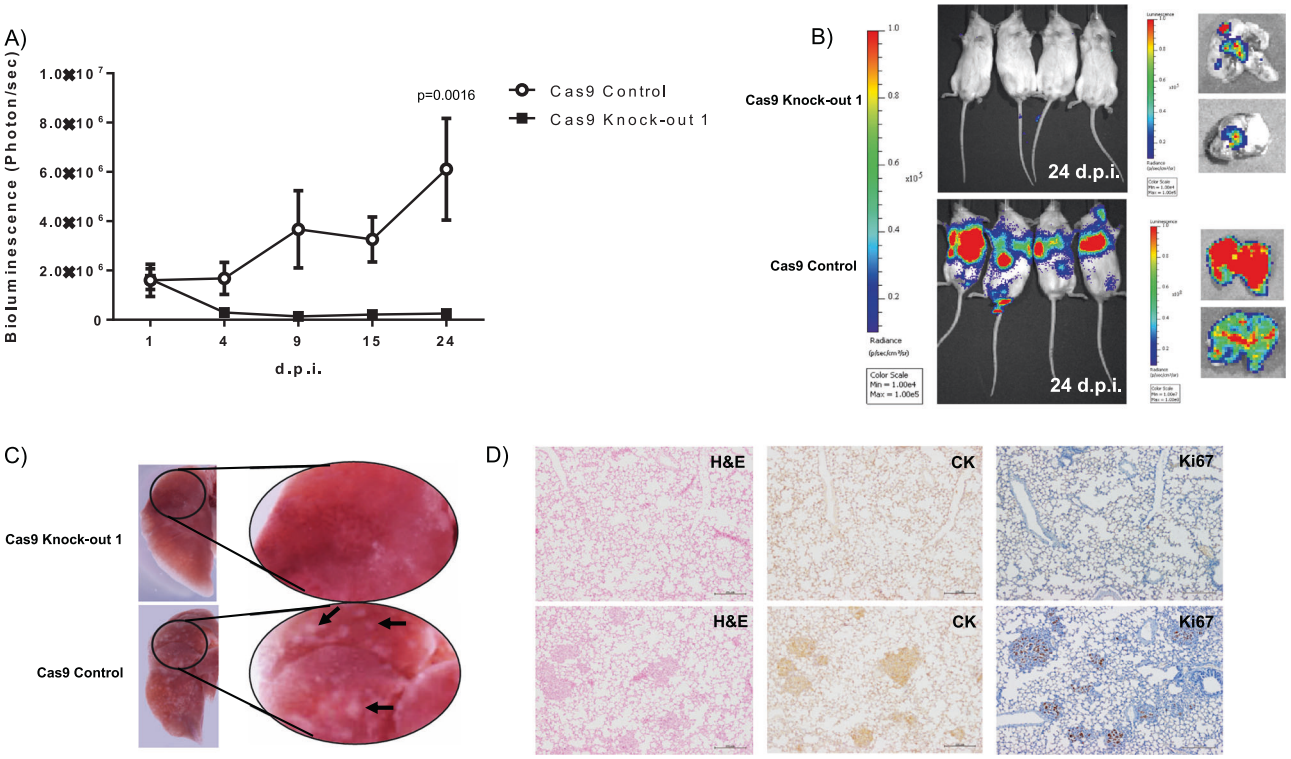

Fig. 4 Tumor xenograft assay of PKP1 knockout cells on immunodeficient NSG mice. a Tumor development tracking at 24 days revealed a lower signal in mice injected with PKP1-knockout vs. PKP1-expressing clones over time ($p = 0.0016$). **b** Luminescence analysis in vivo of mice and ex vivo of extracted organs at 24 days after cell injection, showing that luminescence was mainly observed in lungs and was considerably greater in mice injected with PKP1-expressing clones than in those injected with PKP1-knockout cells, where it was difficult to detect. **c** Macroscopic study of the lung surface, which appears rich on hyperplasic spots (some of them exemplified with arrows) on PKP1-expressing xenografts but relatively smooth, similar to wild-type lung surface, in PKP1-knockout xenografts. **d** Hematoxylin-eosin, antihuman cytokeratin antibody, and antihuman Ki-67 antibody staining results reveal tumor structures in mice injected with PKP1-expressing clones (controls) but not in those injected with PKP1-knockout clones; scale: 200 µm. Cas9 Control, pspcas9(bb)-2a-puro empty vector treated SK-MES-1 clonal cell line; Cas9 Knock-Out 1, pspcas9(bb)-2a-puro sgRNA against PKP1 exon 3 treated SK-MES-1 clonal cell line 1; d.p.i., days post-injection; H&E, hematoxylin and eosin staining; CK; human cytokeratin immunostaining; Ki67, proliferation marker protein Ki-67 immunostaining.

xenografts, which was similar to that in wild-type lungs (Fig. 4c). Lung tissue samples were histologically processed and stained with hematoxylin-eosin, antihuman cytokeratin antibody, and anti-Ki-67 antibody (Fig. 4d). Tumor cells were difficult to detect in stained lung histological preparations of xenografts from mice injected with PKP1-knockout cells but were readily and frequently observed in those derived from mice with PKP1-expressing cells.

Taken together, the above results demonstrate that PKP1 expression is crucial for the correct development and progression of the in vivo xenografts, and that PKP1 expression enhances in vivo tumor growth in SqCLC.

Gene expression profiles after PKP1 depletion reveal a functional relationship between MYC and PKP1

We performed comparative transcriptome profile analysis between SK-MES-1 PKP1-knockdown and their PKP1-expressing controls in order to investigate alternative PKP1 functions related to the oncogenic activity observed in the above assays. Experiments were performed in duplicate in SK-MES-1 cells and scrambled-siRNA served as controls. Adopting the criteria of fold change > 1.5 and $p < 0.05$, 69 genes were found to be differentially expressed (42 up and 27 down), including *PKP1*, which was the most inhibited gene (fold change = −3.09, $p = 0.01$) (Fig. S5).

Next, we used gene set enrichment analysis (GSEA) to search for enriched biological functions and molecular signatures, using the recommended false discovery rate cutoff of <0.25. After thorough examination of the results and the removal of likely false positives (i.e., gene sets with enrichment score peaks for both upregulation and downregulation), we found five MYC-related gene sets to be in the top inhibited hallmarks of cancer. As example, "HALLMARK_MYC_TARGETS_V1" had a normalized enrichment score (NES) of −1.84 (Fig. 5a, b and Table 1). Interestingly, although MYC targets were downregulated,

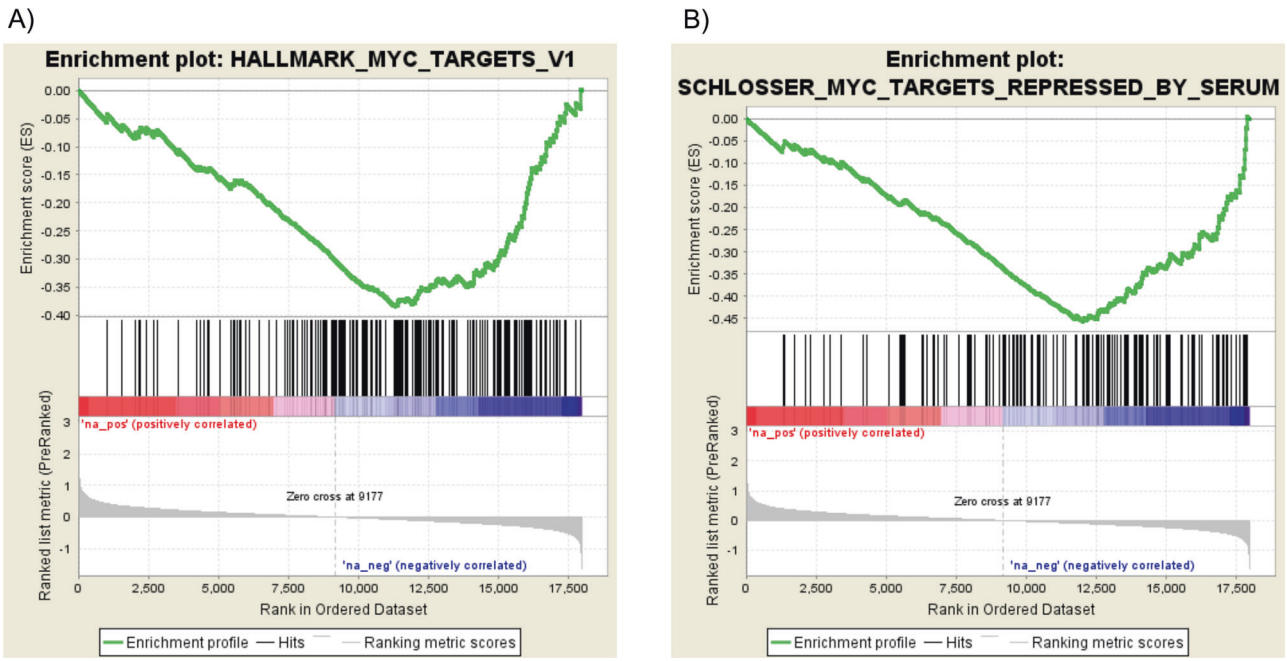

Fig. 5 Top-scoring MYC-related gene sets in a gene set enrichment analysis (GSEA) of the results of the transcriptome profiling in SK-MES-1 PKP1 knockdown cells and their PKP1-expressing controls. a Gene set "HALLMARK_MYC_ TARGETS_V1" was downregulated after PKP1 knockdown. **b** Gene set "SCHLOSSER_-MYC_TARGETS_REPRESSED_BY_SERUM" was also downregulated after PKP1 knockdown.

Table 1 Table displaying the top-scoring MYC-related gene sets alongside their normalized enrichment score (NES) and false discovery rate (FDR); the recommended FDR cutoff of <0.25 was applied

Gene set	NES	FDR
HALLMARK_MYC_TARGETS_V1	−1.84	0.001
SCHLOSSER_MYC_TARGETS_REPRESSED_BY_SERUM	−2.18	0.002
PID_MYC_ACTIV_PATHWAY	−1.94	0.028
KIM_MYC_AMPLIFICATION_TARGETS_UP	−1.75	0.074
SCHUHMACHER_MYC_TARGETS_UP	−1.68	0.107

mRNA levels of *MYC* itself appeared to be unaltered. For this reason, we further explored the relationship between MYC and PKP1, as detailed below.

PKP1 enhances translation of MYC by binding to its 5′UTR

Experiments were then conducted on the relationship between PKP1 and MYC. In line with the aforementioned transcriptome profiling results, qPCR analysis in SK-MES-1 cells showed no significant change in *MYC* mRNA level after PKP1 knockdown (Fig. S6A.1). However, MYC protein levels in SK-MES-1 cells were appreciably reduced by PKP1 knockdown (Fig. 6a), suggesting that PKP1 regulated MYC expression at posttranscriptional level. We extended our results to four additional SqCLC cell lines in different experimental setups (knocking-down PKP1 in EPLC-272H and LUDLU-1, or overexpressing PKP1 in NCI-H520 and NCI-H2170 cell lines).

Importantly, results obtained at the protein (Fig. 6a, b) and mRNA (Fig. S6A.1, A.2) levels strongly supported the PKP1 role in MYC translation in all cases, regardless the experimental setup.

We then attempted to identify partners interacting with PKP1 to explore the direct/indirect mechanism(s) underlying this regulation. Because translation regulation mainly takes place in the cytoplasm, we immunoprecipitated cytoplasmic PKP1, analyzing the proteins pulled down with PKP1 by means of liquid chromatography tandem mass spectrometry (LC–MS/MS). After several attempts, this analysis was not able to detect PKP1 among these proteins, possibly because endogenous PKP1 expression in SK-MES-1 cell line was not sufficient for the antibody used. We therefore decided to use a lung

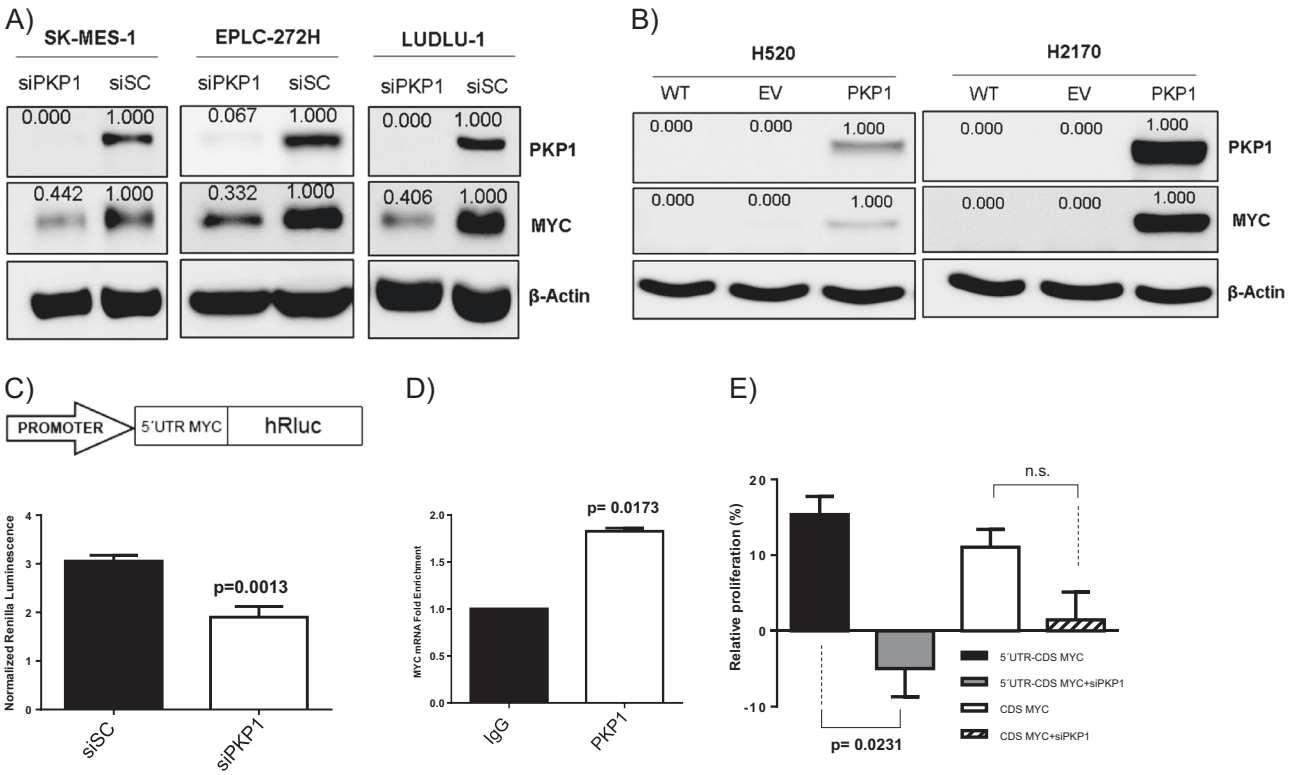

Fig. 6 PKP1/MYC functional relationship. a Western blot assay of PKP1 and MYC protein expression after silencing of PKP1 in three SqCLC cell lines. Reduction in PKP1 induces MYC inhibition. **b** Western blot assay of PKP1 and MYC protein status after PKP1 ectopic expression in two SqCLC cell lines. PKP1 ectopic expression induces MYC translation (**c**) psiCheck2 cloning strategy for luciferase assays on *MYC* 5′UTR and luciferase assays on *MYC* 5′UTR, revealing a significant reduction in luciferase expression ($p = 0.0013$) after PKP1 silencing. Firefly luciferase expression in the same bicistronic psiCheck2 plasmid was used to normalize the signal. **d** Fold enrichment of *MYC* mRNA level after PKP1 RNA immunoprecipitation (RIP). PKP1 antibody pulldown, normalized to IgG antibody pulldown control, has a significant fold enrichment of 1.8 ($p = 0.0173$). **e** Phenotype rescue after 72 h of cell culture (scramble normalized). Significant proliferation phenotype trend change ($p = 0.0231$) was observed after simultaneous 72 h inhibition of *PKP1* mRNA and ectopic expression of a MYC cDNA containing the 5′UTR and the coding sequence, but not in the case that it only contains the coding sequence. PKP1, plakophilin 1; MYC, MYC proto-oncogene; B-Actin, beta-actin. siPKP1, Knockdown combination of siRNA against PKP1; siSC, scrambled-siRNA control; 5′UTR MYC, psiCheck2 plasmid expressing the 5′UTR of MYC; PKP1, immunoprecipitation of plakophilin 1; IgG, immunoprecipitation of negative control; 5′UTR-CDS MYC, *MYC* 5′UTR plus coding sequence plasmid transduction; 5′UTR-CDS MYC + siPKP1, *MYC* 5′UTR plus coding sequence plasmid transduction plus knockdown combination of siRNA against PKP1 treatment. CDS MYC, *MYC* coding sequence plasmid transduction; CDS MYC + siPKP1, *MYC* coding sequence plasmid transduction plus knockdown combination of siRNA against PKP1 treatment; n.s., nonsignificant.

cancer cell line with higher levels of endogenous PKP1 for this purpose, first analyzing PKP1 levels in 14 NSCLC cell lines (Fig. S7A). *PKP1* mRNA expression was significantly higher in SqCLC-derived than adenocarcinoma-derived lung cancer cell lines, as expected. The EPLC-272H cell line, which was finally selected, had appreciably higher *PKP1* levels in comparison with SK-MES-1 and the other tested cell lines. Western blot assays were performed to verify PKP1 protein levels in EPLC-272H as well as in the SK-MES-1 and NCI-H2170 cell lines used in the previous functional studies. Western blot results confirmed that PKP1 was expressed at higher levels in EPLC-272H than in the other analyzed cell lines (approximately fourfold than SK-MES-1), while PKP1 was undetectable in NCI-H2170 (Fig. S7B). Immunoprecipitation and LC–MS/MS on endogenous PKP1 was successful in EPCL-272H, and the pull down with cytoplasmic PKP1 was analyzed with the Proteome Discoverer using the SEQUEST engine. An output of 599 putative cytosolic PKP1-binding partners was obtained after quality filtering (Table S2).

These 599 putative cytosolic PKP1 partners were analyzed using DAVID 6.8 (https://david.ncifcrf.gov/) to identify enriched biological functions (Table S3). In a functional clustering analysis, the highest enrichment score (57.09) was obtained for the cluster that included functions related to cell–cell adhesion, as expected for this desmosomal protein. The second, third, and fourth highest scores, respectively, were obtained for clusters including biological functions related to: ATP binding (enrichment score = 22.56), RNA binding (enrichment score = 16.99), and ribosomes and translation, especially translational initiation (enrichment

score = 16.33). Taken together, these three clusters pointed to a role for cytosolic PKP1 binding partners in translational initiation, binding rRNA and/or mRNA, as well as possible ATP-dependent roles, such as RNA helicase functions. The list of putative PKP1 partners included 38 proteins associated with the Gene Ontology term "translational initiation", which had a Benjamini-adjusted enrichment p value of 2.5×10^{-20}. All of the proteins related to this biological function are listed in Table S4.

Western blot of the protein extract of PKP1 immunoprecipitation confirm the interaction of PKP1 with poly(A) binding protein cytoplasmic 1 (PABP), the top-1 in our list of PKP1 partners, in EPLC-272H cell line (Fig. S7C). According to the above results, PKP1 interacts with the translation initiation complex.

Luciferase assays were then performed on *MYC* 5′UTR to test whether PKP1 is directly involved in the translational initiation of MYC, cloning *MYC* 5′UTR between the promoter and *Renilla* luciferase open reading frame in the psiCheck-2 plasmid. Firefly luciferase expression in the same bicistronic plasmid was used to normalize the transfection (Fig. S7D). Luciferase assay results showed a significant reduction ($p = 0.0013$) in luciferase expression after PKP1 knockdown (Fig. 6c). To attest a direct interaction between PKP1-*MYC* mRNA we performed RNA immunoprecipitation (RIP) assay. A 1.8-fold enrichment indicated a significant direct interaction ($p = 0.0173$) between PKP1 and *MYC* mRNA level (Fig. 6d).

MYC is key in the tumoral phenotype that PKP1 drives

Finally, to evaluate if the observed phenotype on the cells is directed by the functional relationship PKP1-MYC, we decided to measure the PKP1 effects on proliferation in SK-MES-1 cells after transducing MYC with and without its 5′ UTR. Interestingly, the cells transduced with 5′UTR-MYC experimented negative values of cell proliferation when PKP1 is inhibited. However, this effect was not observed when MYC is transduced without its 5′UTR. Importantly, these results indicate that the presence of the 5′UTR in MYC transcript is a determinant factor for the phenotype mediated by PKP1. In addition, we observed nonsignificant changes in proliferation when MYC is transduced without 5′UTR regardless if PKP1 is inhibited. However, the trend in proliferation changes from positive to negative and become significant ($p = 0.0231$) when MYC is transduced with its 5′UTR (Fig. 6e). These results indicated that the phenotype driven by PKP1 is dependent on the presence of the MYC 5′UTR and hence that MYC is key to develop the observed oncogenic phenotype of PKP1.

Taken together, these findings reveal PKP1 as a previously unknown MYC posttranscriptional activator, attributing novel oncogenic functions to cytoplasmic PKP1. Also, our results are indicative that MYC is key in the phenotype mediated by PKP1 throughout its binding to its 5′UTR.

Discussion

The development of high-throughput genomics and transcriptomics technologies has allowed researchers to achieve major advances in the identification of tumor genes altered by mutation or abnormally expressed. Thus, independent studies, using a combination of high-throughput approaches, previously reported that PKP1 is overexpressed in SqCLC [6, 7, 14–16]. Large amounts of descriptive data are now available, and it is necessary to achieve meaningful functional experiments to understand their relevance in the complex puzzle of cancer.

Functionally, PKP1 is best known as a major component of desmosomes [21], which participate in binding cells together in epithelial sheets. Thus, *PKP1* mutations result in fewer and poorly formed desmosomes, and a loss of epidermal integrity responsible for ectodermal dysplasia/skin fragility syndrome (EDSFS) [22]. Desmosomes play an important role in providing strength to tissues that experience mechanical stress, such as epidermis. Accordingly, *PKP1* expression is high in epidermal tissues but relatively low in normal lung tissue, with a median RPKM (Reads per kilobase per million of mapped reads) of 440 (skin epidermis) vs. 1.9 (lung) [23]. From this point of view, it is not unexpected to encounter *PKP1* expression in SqCLC when its expression in normal lung tissue is low or absent. However, given that desmosome activity is lost or disrupted in many tumors [11], decreasing cell adhesion and promoting metastasis [12], the overexpression in lung cancer of PKP1, a component of desmosomes, is a surprising finding.

The levels of *PKP1* expression in squamous cell carcinoma may in part explain its lesser metastasization in comparison with adenocarcinoma, the other major NSCLC subtype [24]. As other members of the armadillo protein family, PKP1 may play different cell functions with possibly opposing effects on cancer development. In addition, PKP1 is present not only in desmosomes but also in the nucleus and cytoplasm [25], and it could therefore have distinct functions in different cell components [9]. Accordingly, we have demonstrated by immunofluorescence a physiological distribution of PKP1 in both, cell lines and cellular models used (Fig. S3A), and our results suggest that desmosomal PKP1 may play a tumor-suppressor role, enhancing cell cohesion, whereas nondesmosomal cytoplasmic PKP1 plays a pro-oncogenic role and promotes cell proliferation, mainly by enhancing MYC expression at posttranscriptional level.

To our best knowledge, this study contributes the first published evidence of a functional interaction between PKP1 and MYC, providing a possible mechanism of cell transformation in which PKP1 is a posttranscriptional activator of MYC. Importantly, our results indicate that the phenotype is driven by PKP1 and it is dependent on the presence of the MYC 5′UTR (Fig. 6e), suggesting also that MYC plays a significant role in this phenotype.

Some clues about the functional role of PKP1 can be derived from reports on human and animal *PKP1*-knockout phenotypes. Thus, humans with homozygous or compound heterozygous *PKP1* mutations develop EDSFS [22], a very rare inherited autosomal recessive syndrome of which only 21 cases have been reported to date [26]. Most phenotypes of this syndrome have been related to the skin. There is no evidence of higher tumor susceptibility among non-PKP1-expressing individuals, while growth retardation and low birth weight are frequent nonskin-related symptoms in individuals with EDSFS. These phenotypical observations suggest that PKP1 may play a more significant role in promoting cell growth than in enhancing cell cohesion, exerting an overall oncogenic effect. In this line, low birth weight and poor weight gain were recently described in *PKP1*-knockout mice alongside fragile skin symptoms, and keratinocytes isolated from these mice showed reduced proliferation rates [27]. Both observations are in agreement with the results of our PKP1-CRISPR-Cas9 xenograft experiments (Fig. 4a–d).

There are also some interesting resemblances between *Myc* and *Pkp1* mouse phenotypes that may in some manner reflect the functional connection between PKP1 and MYC. For example, cells isolated from both knockout mice [27, 28] showed reduced proliferation, and growth of the animals was impaired, with high embryonic and/or neonatal mortality. In particular, mouse embryonic fibroblasts from conditional *Myc* knockout mice showed growth arrest in G0/G1 and a greater susceptibility to apoptosis, as observed in the SK-MES-1 PKP1 knockdown cells (Figs. 1d–g, S2D, E).

It is important to mention that our results may be of clinical relevance. PKP1 appears to be a useful biomarker to differentiate between SqCLC and lung adenocarcinoma (Fig. S1A), the other main NSCLC cancer subtype, in which PKP1 expression levels are not significantly altered [6, 14–16], In addition, PKP1 inhibition may be of potential therapeutic value against SqCLC, given our finding that it can impair the tumor phenotype in vitro (Figs. 1, 3, S2C) and in vivo (Fig. 4). Finally, our discovery of a functional relationship between PKP1 and MYC may open up the possibility of indirectly targeting MYC not only in NSCLC, where is overexpressed in around 70% of tumors [13], but also in other cancers. This is of particular interest, because *MYC* is an oncogene deregulated in most human cancers and is acknowledged as a “most wanted” target for cancer therapy [29]. However, future studies are needed to determine if the conclusions we found in SqCLC tumors can be extended to other tumors or if they are context-dependent.

Materials and methods

Statistical analysis of five external gene expression datasets

Normalized gene expression data in lung cancer and in normal lung from five external sources were downloaded (Table S1). If the expression values were not log2-transformed, they were converted to log2(expression + 1). For microarray data, if there was more than one probe for PKP1, the correlation of the signal intensity values for all probes were confirmed and averaged.

Cell culture

The cell lines mainly used in this study were SK-MES-1 and NIH 3T3, which were cultured in DMEM medium supplemented with 10% FCS; and LUDLU-1, H520, H2170, and EPLC-272H, which were cultured in RPMI-1640 medium supplemented with 10% FCS. L-glutamine as well as antibiotics and antimycotic agents to prevent contamination were added to cell culture media. HEK293T packaging cells used for the production of lentiviral particles were cultured in DMEM medium supplemented with 10% FCS and L-glutamine. All cells were grown in monolayers in appropriate medium and were maintained at 37 °C in an atmosphere of humidified air with 5% CO_2. All cells were obtained from the ATCC collection, except EPLC-272H which was bought to the DSMZ repository. Both companies perform multiplex PCR of minisatellite markers to confirm cell line identity. Arrived cells were carefully expanded and stored in liquid nitrogen. Previously, mycoplasma testing was conducted using the Venor GeM-qEP kit from Minerva Biolabs (#11–9250). As standard procedure to accomplish the experiments, cells were thawed from the previous generated stock and cultured in appropriated conditions not more than 3 weeks. Confluent cultures were split 1:2 to 1:5 every 3–5 days.

PKP1 isoform determination

To study the prevalence of the two splice isoforms of PKP1 (PKP1a and PKP1b) in the cell lines selected as models, PCR reactions specific to each isoform were performed. Specific primers for PKP1b isoform were: PKP1-b forward, 5′-AAAGGGCCACTAGTAGCAGGGTGA-3′ and PKP1-b reverse, and 5′- TCAGGTAGGTGCGGATGG-3′. A pair

of primers was also designed in order to distinguish the expressed isoform according to the amplicon size (161 bp for PKP1a and 224 bp for PKP1b): PKP1-isoform forward, 5′-GCTGGTGCGATGGCAATAGC-3′ and PKP1-isoform reverse, and 5′-CTGGACATAGGCCATGAGGG-3′.

Transfection

Cells were transfected with 7.5 nM of a combination of two siRNAs to target PKP1 (Ambion, #s10580, #s10582), using Lipofectamine RNAiMAX reagent in accordance with the manufacturer's procedure. After 72 h of incubation, the cells were processed for further analysis. As control, Scramble siRNA (siSC; Ambion, #4390843) was used.

Real time-PCR

All PCR reactions involved initial denaturation at 95 °C for 30 s followed by 40 cycles at 95 °C for 15 s and 60 °C for 60 s.

The following specific primers were used for PCR: PKP1 forward, 5′-TCAGCAACAAGAGCGACAAG-3′; PKP1 reverse, 5′-TCAGGTAGGTGCGGATGG-3′; TBP forward, 5′-CACGCCAGCTTCGGAGAGT-3′, TBP reverse, 5′-GGC ACGAAGTGCAATGGTCC-3′; GAPDH forward, 5′-GAA GGTGAAGGTCGGAGTC-3′, GAPDH reverse, 5′-GAA GATGGTGATGGGATTTC-3′; MYC forward, 5′-CCACC AGCAGCGACTCTGAG-3′ and MYC reverse, 5′-CCAGC AGAAGGTGATCCAGAC-3′ (Sigma). Each experiment was run in triplicate. Gene expression was calculated using the 2-ΔΔCt method, and TBP or GAPDH expression was used as a reference value.

Western blot

Briefly, 25 µg of total protein were subjected to 10–12% SDS-PAGE gels, transferred onto PVDF membranes, blocked for 1 h in PBS containing 3% nonfat dry milk and 0.1% Tween, and incubated overnight at 4 °C with primary antibodies (PKP1, Sigma, #HPA027221, 1:250; MYC, Cell Signaling, #5605, 1:1000; β-Actin, Sigma, #A5441, 1:5000; p21, Cell Signaling, #2947, 1:1000; Caspase 3, Cell Signaling, #9662, 1:1000; GAPDH, Sigma, #PLA0302, 1:1000), and then secondary antibodies (anti-rabbit HRP, Dako, #P0448, 1:2000; anti-mouse HRP, Dako, #P0447, 1:1000; anti-Goat HRP, Dako, #P0449, 1:2000) at room temperature for 1 h. Stripping for reprobing was accomplished when required. Chemiluminescence western blotting analysis system IQ Las 4000 (GE Healthcare) was used to get the images. Band quantification was carried out by Plot Lanes tool of ImageJ v1.49c software.

Clonogenic assay

A total of 5×10^2 cells/well were placed in six-well plates and maintained in complete culture medium for 21 days at 37 °C in the presence of 5% CO_2. The colonies were fixed with a solution containing 2% formaldehyde and 0.2% glutaraldehyde in PBS for 1 h at room temperature. Cells were washed in water and stained with 0.1% crystal violet for 10 min at room temperature. All experiments were performed at least twice in triplicate.

Quantitative data were automatically acquired through Li Cor Odyssey 9120 Imaging System on "700 channel" position (Laser Source: solid-state diode laser at 685 nm).

Cell proliferation

Cells were seeded in suitable confluence in 96-well plate and 20 µL of filtered resazurin solution (0.15 mg/ml) (Sigma, R7017) was added to each well in a final volume of 100 µl/well. Cells were incubated at 37 °C in darkness and an atmosphere of humidified air with 5% CO_2 for 4 h, and 30 µL of 3% SDS to each well were added. Fluorescence of each well using a 560 nm excitation/590 nm emission filter set of the GloMax microplate reader (Promega) was recovered. Each assay was performed at least three times in triplicate.

Cell cycle analysis

SK-MES-1 cells were transfected with PKP1 siRNA (siPKP1) or control siRNA (siSC) and harvested after 3 days. Pellets were fixed by adding 1 ml of 70% cold ethanol and incubated at −20 °C for 24–48 h. After incubation, cells were pelleted, washed again with cold PBS, and resuspended in 50 µL of RNase solution (100 µg/ml in PBS) and 200 µL of PI solution (5 µg/ml in PBS) for the staining step. The cells were incubated for 5 min at room temperature in darkness and then analyzed by flow cytometry using a BD FACSCanto II (BD Biosciences). Each assay was performed in triplicate acquiring a minimum of 10,000 events per sample.

Analysis of apoptosis

Apoptosis was evaluated using a FITC Annexin-V Apoptosis Detection Kit I (BD, 556547). Treated cells in six-well plates at 60% of confluence were harvested using trypsin and washed with cold PBS. Then, pellets were processed following the manufacturer's procedure. The samples were then examined by flow cytometry using a BD FACSCanto II (BD Biosciences). Each assay was performed at least in triplicate acquiring a minimum of 10,000 events per sample.

NIH 3T3 focus formation

The NIH 3T3 murine cells were transduced with the pLVX-PKP1A-DDK-IRES-ZsGreen1 overexpression plasmid and the pLVX-IRES-ZsGreen1 empty vector (control plasmid). Then, they were sorted to guarantee around 100% green cells. Positive cells were seeded in a six-well plate at 80% confluence and allowed to grow for 30 days. After that, we proceeded to crystal violet staining and colony quantification following standard procedures.

Ectopic expression of PKP1

To construct pLVX-PKP1A-Myc-DDK-IRES-ZsGreen1, the entire coding region of PKP1 was amplified by RT-PCR from the commercial vector pCMV6-Entry-PKP1A-Myc-DDK (Origene, RC216972). Primers were designed to incorporate an EcoRI and XbaI restriction sites adjacent to a start codon (ATG) and a stop codon (TGA) respectively (EcoRI-PKP1 forward, 5′-TATAGAATTCATGAACCAC TCGCCGCTCAAGACCGCCTTGGCG-3′; PKP1-XBaI reverse, 5′-ATATTCTAGATCACTTATCGTCGTCATC CTTGTAATCCAGGATATCATTTGCTGCCAGATCCT CTTCTGAGATGAG-3′). The digested PCR product was cloned into appropriate sites of pLVX-IRES-ZsGreen1 vector (Clontech, 632187). Transductions were performed according to standard protocols and resulting cells were subjected to further experiments.

CRISPR-Cas9 genome editing

One guide RNA was designed for each of the first three exons of the PKP1 gene using the online tool http://crispr.mit.edu/ (Exon 1: 5′-ACCCTGAGCCACTCCAATCG-3′, Exon 2: 5′-CCTCTAGGTTCCATGTATGA-3′, Exon 3: 5′-CGACCTCTACTGTGACCCAC-3′), and cloned into the plasmid pSpCas9(BB)-2A-Puro (Addgene, #48139) following a protocol previously described [30].

In order to test guide RNA's cutting efficiency, a surveyor assay was performed (Surveyor Mutation Detection Kit, IDT, 706025) in HEK293T cells using the following primers:

surveyor_Exon1_FW, 5′-GTGCCAGAGAGGGACGA AC-3′; surveyor_Exon1_RV, 5′-TAGGTGCGTAGAC CCTGCC-3′; surveyor_Exon2_FW, 5′-TGGGAATG TCGGAATCCTGC-3′; surveyor_Exon2_RV, 5′-GGTGCC GGTTTTCTCCACTA-3′; surveyor_Exon3_FW, 5′-AT GGCTCAGGTTCCTTCCAC-3′ and surveyor_Exon3_RV, 5′-GCAGTCAGGCTAAGGGTGTG-3′.

Selected plasmid was transfected in the SK-MES-1 cell line and submitted to puromycin selection and clonal expansion. PKP1 knockout of each clone was confirmed by Sanger sequencing and western blot.

Scratch assay

Cells were cultured on a six-well plate until 90% confluence in monolayers in appropriate medium for 24 h. Later, cells were refreshed with restricted medium contained 1% of FCS and wounds were made using a yellow pipette tip. Three wounds per well were made for each sample. Cells were incubated 24 h. Each assay was performed at least in triplicate. Wound healing area was measured by the ImageJ v1.49c software applying the plugin "MRI Wound Healing Tool" at zero time and after 24 h post wound generation.

Immunofluorescence preparations

Seeded cells were fixed with paraformaldehyde 4% in 1× PBS for 7 min at room temperature and permeabilized using 0.5% Triton X-100 in 1× PBS, for 5 min. The blocking step was performed with 3% BSA in PBS at room temperature for 1 h. Primary antibody (diluted in blocking solution) was incubated in a humid chamber at 4 °C overnight. The secondary antibody was incubated following the same procedure, and at room temperature for 1 h. Preparations were incubated with a 1:5000 DAPI dilution form a 1 µg/µl stock for 5 min and placed on microscope slides with mounting medium (Invitrogen ref S36938) and dried at room temperature. The following antibodies were used:

	Name	Dilution	Reference
Primary antibody	PKP1	1:150	Sigma, HPA027221
Secondary antibody	Anti-rabbit ALEXA 488	1:500	Fisher, A-21206
	Anti-rabbit ALEXA 647	1:500	Fisher, A-32733

Live-cell imaging

Treated SK-MES-1 cells seeded in suitable confluence in poly-L-Lysine 8-chambered coverslips (IBIDI, 80824) were imaged by Differential Interference Contrast. Images were acquired using an EC Plan-Neofluar 10× (numeric aperture, 0.3) objective every 30 min during 12–16 h total time. To test cell viability, PI staining was also performed. All experiments were performed with a laser confocal microscope (Zeiss LSM 710) equipped with a stage incubator

with both, temperature and CO_2 control. ZEN software (Zeiss) was used for image analysis.

Monitoring by IVIS of tumor development in mice after injection of tumor cells through the tail vein

The mouse models were generated and housed in the animal facility at University of Granada. The animal work was covered under protocol 17/07/2017/095, which was approved by the Institutional Animal Care and Use Committee of Granada University.

Twenty immunodeficient NSG male 8-week-old mice were separated into two groups (Treatment and Control) and injected though the tail vein with SK-MES-1 PKP1 knockout clone #1 cells (Cas9 knockout 1) or SK-MES-1 clone cells with an empty cassette for the sgRNA (Cas9 Control), respectively.

Experimental and control cells were previously transduced with luciferase (pUltra-chili-luc, Addgene, #48688). Equivalent transfection efficiency was confirmed by flow cytometry using the dTomato reporter and in vivo tumor evolution was tracked thanks to firefly luciferase expression.

Experimental and control groups (ten mice each) were tail-vein injected with 0.2 million cells per 100 µL resuspended in PBS. Cell counting was achieved through inverted microscope and Neubauer Chamber, using Trypan Blue 0.4% solution to assess cell viability for calculations.

Tumor cell distribution and tumor evolution was followed by in vivo luminescence using the IVIS SPECTRUM system (Caliper Life Sciences, 68 Elm Street Hopkinton, MA 01748, USA) in "automatic" at days: 0, 1, 4, 9, 15, and 24. For that purpose, each group was injected intraperitoneally with luciferin (3 mg/100 µL for mice weighing 20 g) and images were taken 3 min later.

At day 24, the two groups of mice were sacrificed, their organs were extracted and their luminescence was measured ex vivo. Finally, all organs were macroscopically analyzed under a magnifying glass and preserved in 4% formaldehyde for further experiments.

Hematoxylin-eosin staining and detection of specific markers of human cells

In order to detect the human-derived tumor masses under the optical microscope, lungs extracted from mice injected with PKP1 knockout clone #1 and from mice injected with PKP1 expressing control clone were fixed in 4% formaldehyde and histologically processed for hematoxylin-eosin staining, immunohistochemistry analyses against human cytokeratin antibody (DAKO #M3515) and against human Ki67 antibody (DAKO #M7240). All these procedures were performed using standardized protocols from Atrys Health S.A.

Transcriptome profiling

Three SK-MES-1 siPKP1 biological replicates and three siSC were prepared for transcriptome profiling. Total RNA was extracted using the mirVana commercial kit (Thermo Fisher Scientific, AM1561). Biotinylated cRNA was hybridized against the HumanHT-12 v4 Expression BeadChip array (Illumina) following the standard Illumina protocols. Samples were randomized before hybridization. The accession number of the transcriptome data is: GSE106770. Raw data from the gene expression microarray were analyzed using R (version 3.2.3) with the packages "limma" and "RankProd" from Bioconductor (https://www.bioconductor.org). The differential expression was considered statistically and biologically significant if FDR < 0.05 and fold change > 1.5 (up or down).

Gene Set Enrichment Analysis (GSEA; http://software.broadinstitute.org/gsea) was used to analyze enriched pathways and biological functions among the differentially expressed genes. Gene sets with FDR < 0.25 and $p < 0.05$ were considered significant.

Luciferase assay

The *MYC* 5′UTR was cloned between the promoter and *Renilla* luciferase open reading frame in the psiCHECK™-2 vector (Promega, C8021). A conventional restriction enzyme cloning strategy with NheI enzyme was followed. *MYC* 5′UTR from genomic DNA was amplified with the following primers including the NheI enzyme restriction sequence: FW_MYC_5UTR_NHEI, 5′-ATATATGCTAGCGACCCCCGAGCTGTGCTG-3′; and RV_MYC_5UTR_NHEI, 5′-ATATATGCTAGCCGTCTAAGCAGCTGCAAGGAG-3′. Firefly luciferase expression present in the same bicistronic plasmid was used to normalize the transfection. PKP1 was inhibited as previously described.

Co-immunoprecipitation

Separation of the cytoplasmic and nuclear fractions and co-immunoprecipitation were performed following a previously described protocol [31] with slight modifications.

The samples were cleaned-up, digested, separated by UPLC chromatography and analyzed, on a Thermo Orbitrap Fusion (Q-OT-qIT, Thermo Fisher Scientific), by the Proteomics Facility at Research Support Central Service at University of Cordoba (Spain) following standardized protocols.

They also processed the raw data using Proteome Discoverer (version 2.1.0.81, Thermo Fisher Scientific). In our laboratory, a final list of filtered proteins was analyzed using the functional clustering analysis tool in DAVID 6.8 (https://david.ncifcrf.gov/).

RNA immunoprecipitation (RIP)

RNA immunoprecipitation was performed in the EPLC-272H cell line in duplicate using the Magna RIP Kit (Merk-Millipore. 17–700) as described in the supplied "Detailed protocol". One RIP reaction (one immunoprecipitation using one antibody) required 100 µL of cell lysate from 2×10^7 cells. Total RNA extraction was performed using TRIzol reagent (Invitrogen. Ref: 15596026). *MYC* mRNA level after PKP1 and IgG antibody pulldown was determined by qPCR using the previous described primers. Finally, the data normalization method used was the called "signal over background" or "relative to the no-antibody control". RIP signals were divided by the no-antibody signals, representing the RIP signal as the fold increase in signal relative to the background signal.

Statistical analyses

The results are expressed as mean ± S.D. and represent at least two experiments. Statistical differences were analyzed using paired, two-tailed *t*-tests. Significance was considered when $p < 0.05$.

Data availability

The microarray data have been deposited on Gene Expression Omnibus (GEO) under the accession number GSE106770.

Acknowledgements We thank to PhD program in Biochemistry and Molecular Biology of University of Granada and to Montse Sanchez-Céspedes for the critical read of the paper.

Funding JM-P and LB were supported by fellowships from Fundación Anticancer San Francisco Javier y Santa Cándida/UGR. AA was supported by a PhD FPU fellowship (FPU17/00067). PP was supported by a PhD "La Caixa Foundation" LCF/BQ/DE15/10360019 Fellowship. IFC was supported by a PhD FPI-fellowship (BES-2013-064596). JCA-P is supported by a Marie Sklodowska Curie action (H2020-MSCA-IF-2018). CB and MIR were supported by Consejería de Sanidad de la Junta de Andalucía (Pl-0245-2017). MEF-V was supported by Junta de Andalucía (PAIDI CTS-303). PPM laboratory is funded by the Ministry of Economy of Spain (SAF2015-67919-R), Junta de Andalucía (P12-BIO-1655, PAIDI CTS-993), Francisco Cobos Foundation, FERO foundation, International Association for the study of lung cancer (IASLC) and Fundación Científica de la Asociación Española Contra el Cáncer (Lab AECC-2018). The funders had no role in study design, data collection and analysis, decision to publish, or preparation of the paper.

Author contributions JM-P, LB, MIR, ID-C, PP, CB, IFC, JCA-P performed and validated the experimental data. AA performed most of the bioinformatics and statistical analysis. PPM provided conceptualized the work, designed the experiments, supervised the experiments, provided expertize and feedback, structured the results, and wrote the first draft of the paper. MEF-V reviewed the paper and provided some supervision of the experiments. MEF-V and PPM participated in the funding acquisition and project administration.

Compliance with ethical standards

Conflict of interest The authors declare that they have no conflict of interest.

Ethical approval This project has been approved by the institutional ethical committee of the University of Granada.

Publisher's note Springer Nature remains neutral with regard to jurisdictional claims in published maps and institutional affiliations.

References

1. Bender E. Epidemiology: the dominant malignancy. Nature. 2014;513:S2. https://doi.org/10.1038/513S2a.
2. Bray F, Ferlay J, Soerjomataram I, Siegel RL, Torre LA, Jemal A. Global cancer statistics 2018: GLOBOCAN estimates of incidence and mortality worldwide for 36 cancers in 185 countries. CA Cancer J Clin. 2018;68:394–424. https://doi.org/10.3322/caac.21492. Epub 12 Sep 2018.
3. Molina JR, Yang P, Cassivi SD, Schild SE, Adjei AA. Non-small cell lung cancer: epidemiology, risk factors, treatment, and survivorship. Mayo Clin Proc. 2008;83:584–94. http://www.ncbi.nlm.nih.gov/pubmed/18452692.
4. Collisson EA, Campbell JD, Brooks AN, Berger AH, Lee W, Chmielecki J. Comprehensive molecular profiling of lung adenocarcinoma. Nature. 2014;511:543–550. https://doi.org/10.1038/nature13385. Epub 9 July 2014.
5. Kim HR, Shim HS, Chung JH, Lee YJ, Hong YK, Rha SY. Distinct clinical features and outcomes in never-smokers with nonsmall cell lung cancer who harbor EGFR or KRAS mutations or ALK rearrangement. Cancer. 2012;118:729–739. https://doi.org/10.1002/cncr.26311. Epub 30 June 2011.
6. Angulo B, Suarez-Gauthier A, Lopez-Rios F, Medina PP, Conde E, Tang M. et al. Expression signatures in lung cancer reveal a profile for EGFR-mutant tumours and identify selective PIK3CA overexpression by gene amplification. J Pathol. 2008;214:347–56. https://onlinelibrary.wiley.com/doi/abs/10.1002/path.2267.
7. Sanchez-Palencia A, Gomez-Morales M, Gomez-Capilla JA, Pedraza V, Boyero L, Rosell R, et al. Gene expression profiling reveals novel biomarkers in nonsmall cell lung cancer. Int J Cancer. 2011;129:355–64. https://onlinelibrary.wiley.com/doi/abs/10.1002/ijc.25704.
8. Perez-Moreno P, Brambilla E, Thomas R, Soria JC. Squamous cell carcinoma of the lung: molecular subtypes and therapeutic opportunities. Clin Cancer Res. 2012;18:2443–2451. https://doi.org/10.1158/1078-0432.CCR-11-2370. Epub 8 Mar 2012.
9. Hatzfeld M. Plakophilins: multifunctional proteins or just regulators of desmosomal adhesion? Biochim Biophys Acta. 2007;1773:69–77. http://www.sciencedirect.com/science/article/pii/S0167488906000954.
10. Krunic AL, Garrod DR, Madani S, Buchanan MD, Clark RE. Immunohistochemical staining for desmogleins 1 and 2 in keratinocytic neoplasms with squamous phenotype: actinic keratosis, keratoacanthoma and squamous cell carcinoma of the skin. Br J Cancer. 1998;77:1275–9. https://www.ncbi.nlm.nih.gov/pubmed/9579833.
11. Dusek RL, Attardi LD. Desmosomes: new perpetrators in tumour suppression. Nat Rev Cancer. 2011;11:317. https://doi.org/10.1038/nrc3051.

12. Kundu ST, Gosavi P, Khapare N, Patel R, Hosing AS, Maru GB, et al. Plakophilin3 downregulation leads to a decrease in cell adhesion and promotes metastasis. Int J Cancer. 2008;123:2303–14. https://onlinelibrary.wiley.com/doi/abs/10.1002/ijc.23797.
13. Richardson G, Johnson BE. The biology of lung cancer. Semin Oncol. 1993;20:105–27.
14. Bhattacharjee A, Richards WG, Staunton J, Li C, Monti S, Vasa P, et al. Classification of human lung carcinomas by mRNA expression profiling reveals distinct adenocarcinoma subclasses. Proc Natl Acad Sci. 2001;98:13790–5. https://www.pnas.org/content/98/24/13790.
15. Hou J, Aerts J, den Hamer B, van IJcken W, den Bakker M, Riegman P, et al. Gene expression-based classification of non-small cell lung carcinomas and survival prediction. PLoS ONE. 2010;5:1–12. https://doi.org/10.1371/journal.pone.0010312.
16. TCGA Research Network. 2018. https://cancergenome.nih.gov/.
17. Furukawa C, Daigo Y, Ishikawa N, Kato T, Ito T, Tsuchiya E, et al. Plakophilin 3 oncogene as prognostic marker and therapeutic target for lung cancer. Cancer Res. 2005;65:7102–10. http://cancerres.aacrjournals.org/content/65/16/7102.
18. Schmidt A, Langbein L, Rode M, Prätzel S, Zimbelmann R, Franke W. Plakophilins 1a and 1b: Widespread nuclear proteins recruited in specific epithelial cells as desmosomal plaque components. Cell Tissue Res. 1997;290:481–99.
19. Clark GJ, Cox AD, Graham SM, Der CJ. Biological assays for Ras transformation. Methods Enzymol. 1995;255:395–412. https://doi.org/10.1016/s0076-6879(95)55042-9.
20. Liang C-C, Park AY, Guan J-L. In vitro scratch assay: a convenient and inexpensive method for analysis of cell migration in vitro. Nat Protoc. 2007;2:329. https://doi.org/10.1038/nprot.2007.30.
21. Hatzfeld M, Haffner C, Schulze K, Vinzens U. The function of plakophilin 1 in desmosome assembly and actin filament organization. J Cell Biol. 2000;149:209–22. https://www.ncbi.nlm.nih.gov/pubmed/10747098.
22. McGrath JA, McMillan JR, Shemanko CS, Runswick SK, Leigh IM, Lane EB, et al. Mutations in the plakophilin 1 gene result in ectodermal dysplasia/skin fragility syndrome. Nat Genet. 1997;17:240. https://doi.org/10.1038/ng1097-240.
23. Consortium Gte. The Genotype-Tissue Expression (GTEx) project. Nat Genet. 2013;45:580–5. https://www.ncbi.nlm.nih.gov/pubmed/23715323.
24. Budczies J, von Winterfeld M, Klauschen F, Bockmayr M, Lennerz JK, Denkert C, et al. The landscape of metastatic progression patterns across major human cancers. Oncotarget. 2015;6:570–83. https://www.ncbi.nlm.nih.gov/pubmed/25402435.
25. Gomez-Morales M, Camara-Pulido M, Miranda-Leon MT, Sanchez-Palencia A, Boyero L, Gomez-Capilla JA, et al. Differential immunohistochemical localization of desmosomal plaque-related proteins in non-small-cell lung cancer. Histopathology. 2013;63:103–13. https://www.ncbi.nlm.nih.gov/pubmed/23711109.
26. Alatas ET, Kara A, Kara M, Dogan G, Baysal O. Ectodermal dysplasia-skin fragility syndrome with a new mutation. Indian J Dermatol Venereol Leprol. 2017;83:476–9. https://www.ncbi.nlm.nih.gov/pubmed/28540868e.
27. Rietscher K, Wolf A, Hause G, Rother A, Keil R, Magin TM, et al. Growth retardation, loss of desmosomal adhesion, and impaired tight junction function identify a unique role of plakophilin 1 in-vivo. J Invest Dermatol. 2016;136:1471–8. https://doi.org/10.1016/j.jid.2016.03.021.
28. Pirity M, Blanck JK, Schreiber-Agus N. Lessons learned from Myc/Max/Mad knockout mice. Curr Top Microbiol Immunol. 2006;302:205–34. https://www.ncbi.nlm.nih.gov/pubmed/16620030.
29. Whitfield JR, Beaulieu M-E, Soucek L. Strategies to Inhibit Myc and Their Clinical Applicability. Front cell Dev Biol. 2017;5:10. https://www.ncbi.nlm.nih.gov/pubmed/28280720.
30. Ran FA, Hsu PD, Wright J, Agarwala V, Scott DA, Zhang F. Genome engineering using the CRISPR-Cas9 system. Nat Protoc. 2013;8:2281–308. https://www.ncbi.nlm.nih.gov/pubmed/24157548.
31. Munoz WA, Lee M, Miller RK, Ahmed Z, Ji H, Link TM. Plakophilin-3 catenin associates with the ETV1/ER81 transcription factor to positively modulate gene activity. PLoS ONE. 2014;9:e86784. https://doi.org/10.1371/journal.pone.0086784. eCollection 2014.